International Journal of Mathematical Analysis and Applications
2014; 1(5): 73-79
Published online November 30, 2014 (http://www.aascit.org/journal/ijmaa)
ISSN: 2375-3927

Keywords
Bump,
Compressible Flow,
Mach Number,
Static Pressure

Received:October 10, 2014
Revised: November 26, 2014
Accepted: November 27, 2014

Numerical analysis of two-dimensional isentropic compressible flowinside a channel with circular arc and rectangular bump

Amir Hassanzadeh[1, *], Nasser Mostafavinia[1], Reza Esmaily[1], Nader Pourmahmoud[2]

[1]Departmentof Mechanical Engineering, Sama Technical and Vocational College, Mahabad Branch, Islamic Azad University, Mahabad, Iran
[2]Department of Mechanical Engineering, Faculty of Engineering, Urmia University, Urmia, Iran

Email address
amir.info@gmail.com (A. Hassanzadeh)

Citation
Amir Hassanzadeh, Nasser Mostafavinia, Reza Esmaily, Nader Pourmahmoud. Numerical Analysis of Two-Dimensional Isentropic Compressible FlowInsidea Channel with Circular Arc and Rectangular Bump. *International Journal of Mathematical Analysis and Applications.* Vol. 1, No. 5, 2014, pp. 73-79.

Abstract
In this article, 2-dimensional isentropic compressible flow throughout a rectangular channel with a bump is studied numerically. The recent researches were often carried out for a circular arc bump of 4 or 10% of total height of channel. In the present study the influence of geometry of bump in the channel is investigated. Due to this aim, two kinds of bump (circular arc and rectangular) with the height of 10, 30 and 50% of total height of channel are investigated and the obtained results are compared. The inlet Mach number is 0.5 for all the CFD models. The governing equations are Euler equations and a Finite Volume method is applied to the equations in order to solve them. Some of the results are compared to the valid available data and they show reasonable agreement. The Mach number and static pressure distributions inside the channeltogether with secondary flow investigation are the main results of the article.

1. Introduction

The study of isentropic compressible flow over a bumpis a popular scheme of Computational Fluid Dynamics (CFD). The previous studies were often done for the 4 or 10% circular arc bump. Different CFD methods together with different inlet Mach numbers have been studied whiten recent years for this case of study. Mallet [1] used the Finite Volume method to solve the problem. Shapiro [2] investigated the flow with the Mach number of 1.4 and Le Beau [3] surveyed awider range of inlet Mach numbers. Djavareshkian[4]utilized NVD method for analyzing 10% circular arc bump. He performed his researches for subsonic, transonic and supersonic flows. His results were valid for fairly coarse meshes. Rizzi[5] investigated 4.2% bump and Veress[6]confirmed the Rizzi's [5] results using Finite Volume method. Sandham et al. [7] used LES turbulence model in order to study a turbulent flow over a bump. Chiocchia and Gabutti[8] introduced a mathematical model for solving the equations for flow over a bump. Wong et al. [9] tested a 3D model equipped with a bump in order to control the shock waves experimentally and numerically.

The literature review shows that bump problem is usually benefited as a case study for validating a new numerical method but seldom analyses of the flow manner inside the channel has been considered as a main goal. In the present article, the influence of geometry of the bump on the flow field manner is investigated numerically. Two kinds of bumps including circular arc and rectangular shapes with a height of 10, 30 and 50% of total height of channelare analyzed. The results are being validated for the case of 10% circular arc bump using the results of Darwish and Moukalled[10].

2. Model Description and Boundary Conditions

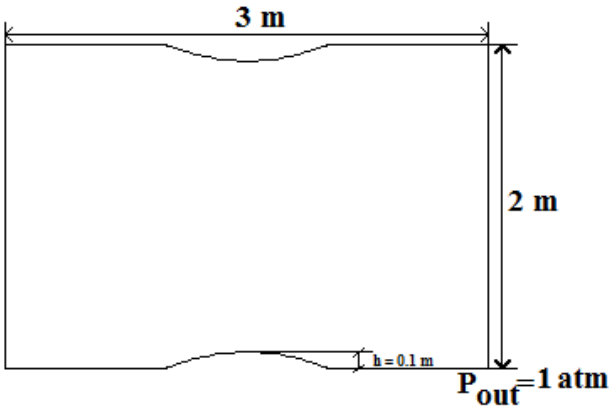

Fig 1. *Physical configuration and dimensions of problem*

Figure 1 displays the geometry of problem. The compressed and steady air passes through the a rectangular channel which its height is 2 m and there is a 10% reduction of cross section area(10% flow blockage) in the middle of the channel. The length of channel is considered 3 m. Air flows through the channel from left to right. At the inlet boundary, it is assumed that air at a static temperature T of 287.7K is entering with a velocity of 170 m/s. The absolute static discharge pressure P_{out} at the exit boundary is assumed to be 10^5Pa which is a pressure of about one atmosphere. The speed of sound, a, in air is obtained from the following expression,

$$a = \sqrt{\gamma RT / M} \tag{1}$$

where $\gamma = c_p / c_v = 1.4$ is the ratio of the specific heats, $\overline{R} = 8314$ J/(kgmol K) is the universal gas constant, and M = 28.966 (kg/kgmol) is the molecular weight of air. The above data implies that at the inlet boundary Ma = 0.5.If we consider the following constant air properties:

- Viscosity; $\mu = 1.8 \times 10^{-5}$ kg/(m-s)
- Specific heat at constant pressure; c_p= 1004 J/(kg-K)

and used the ideal gas equation then the governing equation ofthe density, ρ, in the present example is thus

$$\rho = \frac{pM}{\overline{R}T} \tag{2}$$

The above defined parameters lead to flow Reynolds number of, Re = 1.14×10^6 based on inlet conditions and exit pressure. The large values ofthis dimensionless parameter combined in the fact that the walls of the channel arebeing modeled as insulated and frictionless means that the flow process being simulated isessentiallyinviscid.

At the lower wall, a no-slip condition was used for the velocity components and an isothermal wall condition was prescribed. At the upper surface, a free-slip boundary condition was applied.

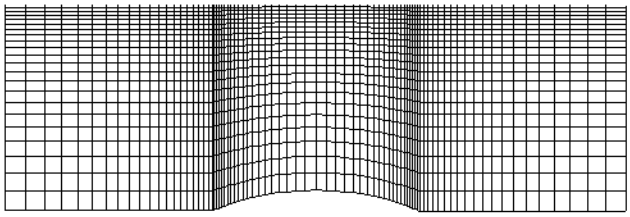

Fig 2. *Typical computational grid and boundary condition*

The computational mesh comprises of 3200 elements; 80 along the length of the channel and 40 across the channel height. Figure 2 illustrates the half of generated mesh along with boundary conditions.

3. Governing Equations

When, however, the Reynolds number is sufficiently high, of the order of 10^5 or more, viscosity effects usually are of importance to the flow only in the boundary layer near a body or a wall or possibly in confined regions in the wake of a body. In many problems, such as the case of waves on a free surface, viscosity effects may be of secondary importance in most of the flow field.In solving such flows, it is convenientandusefulto first omit viscosity termscompletely. Thus the Euler equation is used here [11]. In addition to the momentum and continuity equations, the energy equation also needs to be solved. The simulation ofcompressible steady Newtonian fluid under isothermal conditions may be consideredas follows:

$$\frac{\partial \rho}{\partial t} + \nabla.(\rho V) = 0 \tag{3}$$

$$\rho \frac{dV}{dt} - \rho g + \nabla p = 0 \tag{4}$$

$$\frac{\partial (T)}{\partial t} - \frac{1}{\rho c_p} \nabla.(pV) = 0 \tag{5}$$

4. Numerical Procedure and Validation

A home-generated FORTRAN code based on the Finite Volume method using the SIMPLE algorithm has been developed to solve the governing equations. The discretized equations have been solved using a strongly implicit procedure (SIP). The graphical figures have been created by Tecplot program. In order to substantiate the accuracy of the present computational code, the results of Mach number distributionin the center line and wall obtained from the present code is compared with the numerical results of Darwish and Moukalled[10]. Figure 3 shows this comparison where the variations of the Mach number have been depicted along the centerline and wall of the channel for the model with 10% arc circular bump. It should be noted that, these results have been obtained for Ma =0.5 and the same geometry as used in the reference of [10]. As it can be seen, a reasonable agreement has been found between the current simulation and the numerical results of Darwish and Moukalled[10] implying the accuracy of the present code.

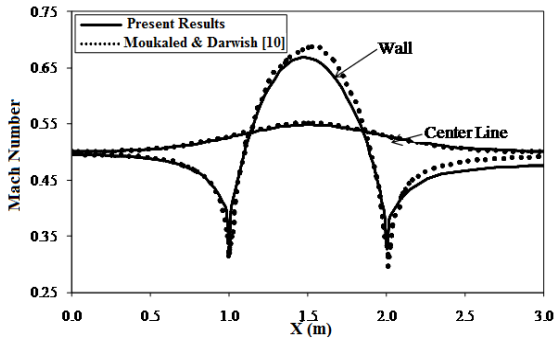

Fig 3. *Mach number distribution along the centerline and wall of channel with 10% arc circular bump*

5. Results

5.1. Mach Number and Static Pressure Investigation

Generally, there can be various possible arrangements for bump geometry with different inlet Mach numbers and sizes of channel. In the present work, two kinds of arc circular and rectangular with various heights and with inlet Mach = 0.5 (subsonic flow) are considered, so that all the cases are symmetric about the centerline of channel. For ease of analysis of the results, only the bottom half of channel is presented. The main goal of this article is to study the effect of geometrical arrangement of bump on the flow fieldbehavior within the channel.

Figure 4 shows the iso-Mach lines throughout the channel for different models.The numerical solution for arc circular bumps is more symmetric about the mid chord than the rectangular ones. For circular models, the Mach number on the top of the bump is greater than the edges of bumpand it how the acceleration of the flow over the circular bump but for rectangular models, the Mach number on the front of the bump is greater than the top and back of bump.The Mach number values for the 30% arc circular bum are somewhat greater than the other models but for rectangular models, the model with 10% bump has the stronger shock waves. The symmetry of iso-Mach lines decreases by increase of bump height and it is more evidence in the circular models. Every circular model has stronger Mach waves than its similar rectangular model. For 30 and 50% arc circular models, the Mach number approaches to an amount of somewhat greater than 1 (maximum 1.13) and it increases the chance of shock layers creation. The existence of circular bump in the middle of the channel helps the flow to speed up in the middle of channel.

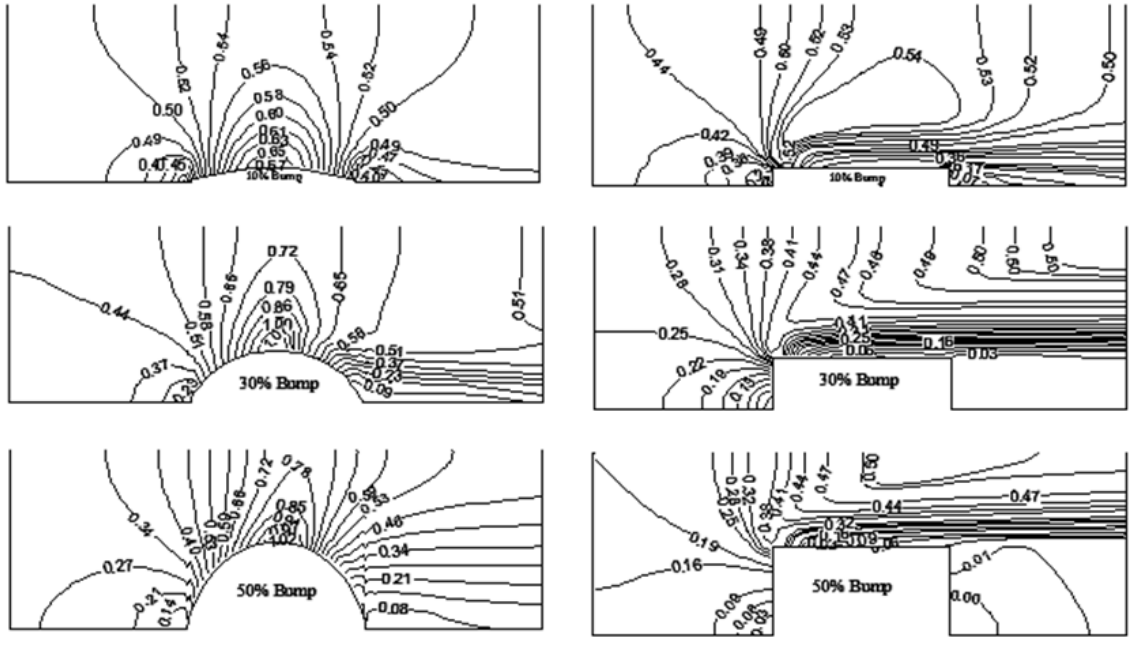

Fig 4. *Iso-Mach number lines inside models with different bumps*

The Mach number distribution along the centerline and the lower wallhas been displayed in fig. 5 and 6. According to fig. 5a, the Mach number is Maximum in the middle of the channel for model of 10%. As the height of channel increases, the location of pick point for Mach number in the centerline tends to the left side however it is not significant. The symmetry of Mach number distribution in the centerline is completely evidence for the model of 10% arc circular bump but the symmetry disturb due to increasing bump height. The maximum amounts of Mach number in the centerline are 0.55, 0.70 and 0.78 for the models of 10%, 30% and 50% respectively. Figure 5b, displays the Mach number distribution along the centerline of channel for rectangular bump models. None of the models has symmetry for this case. The exit Mach number in the center of channel decreases as the height of bump increases.The maximum amounts of Mach number in the centerline are 0.54, 0.50 and 0.51 for the models of 10%, 30% and 50% respectively. The exit Mach numbers for models equipped with circular bumps is higher than rectangular ones and it reveals the advantage of using circular bumps over rectangular bumps.

Figure 6a represents the Mach number distribution along lower wall of channel for rectangular bump models. For all 3 models, the Mach number drops in the start point and end point of bump however it rises in the middle of bump. The symmetry of Mach number distribution is lower for the models with 30% and 50%circular bump respect to 10% model. The maximum amounts of Mach number along the lower wall of channel are 0.67, 1.14 and 1.04 for the models of 10%, 30% and 50% respectively. For rectangular models, the maximum Mach number occurs in the front of bump as shown in fig. 6b.In the front section of rectangular bump (X = 1 m) the Mach number decreases suddenly and then increases dramatically.The maximum amounts of Mach numbers for rectangular models along the wall are smaller than arc circular ones.

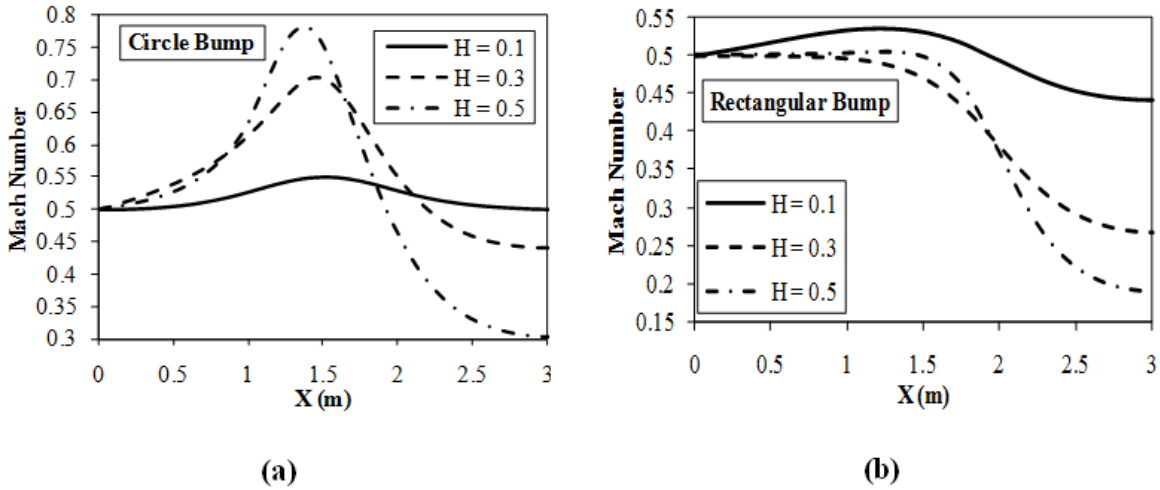

Fig 5. *Mach number distribution along centerline of channel for a)circular bums b)rectangular bumps*

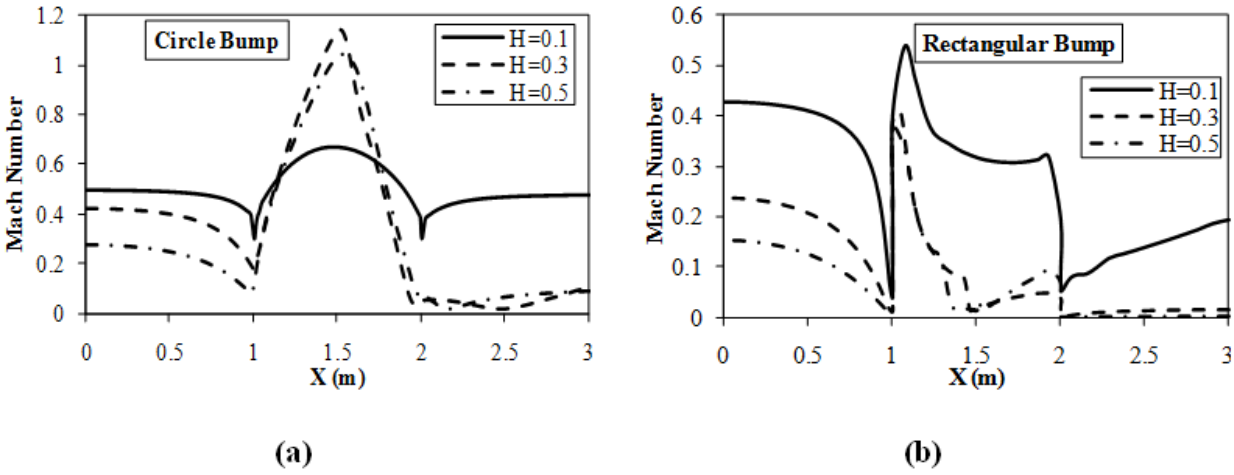

Fig 6. *Mach number distribution along lower wall of channel for a)circular bums b)rectangular bumps*

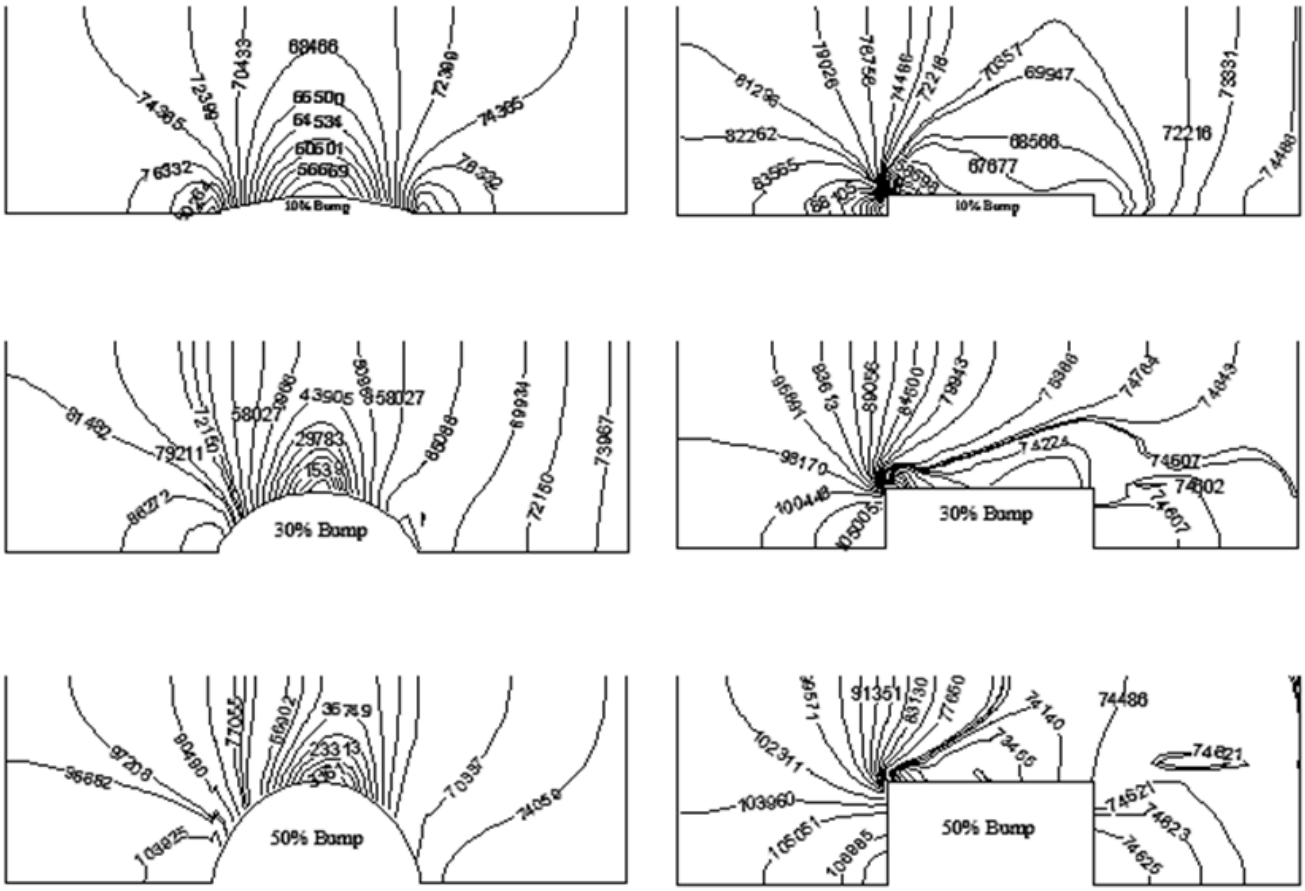

Fig 7. *Iso-bar lines inside models with different bumps*

The static pressure contour (iso-bar lines) for different models has been depicted in fig. 7. The description of static pressure distribution throughout the channel is almost similar to Mach number. Even, the total behavior of contours is the same for Mach number and static pressure in every case of study.Namely, where the Mach number is high, the static pressure is high too and so on. Thus explanation of this figure is not presented in details for brevity.

5.2. Secondary Flow

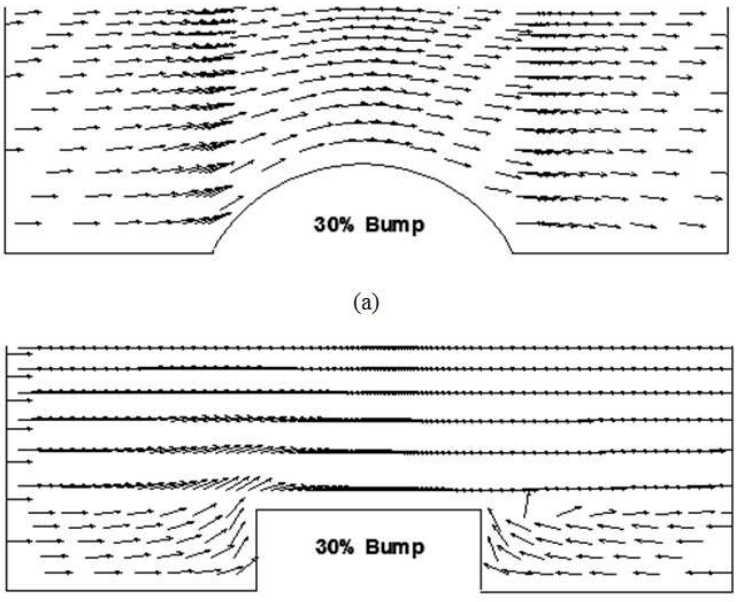

(a)

(b)

Fig 8. *Velocity vector within the channel with a) 30% arc circular bump b) 30% rectangular bump*

The velocity victor and streamlines inside the channel and specially near the bump can be an interesting point of view. Figure 8 displays velocity victors in the channel with 30% arc circle channel. As it can be seen the air passes the channel normally and no one can see any special or strange phenomenon near the bump (fig. 8a). But, in fig 8b one can see the reversed flow on the back region of the bump and it causes to creation of secondary flow. Thissecondary flow had to be captured, and it can be seen that a region of recirculationsecondary flow is present within the channel, as can be seen in fig. 9b and a zoomed view of fig. 9c for a sample model of 30% bump.

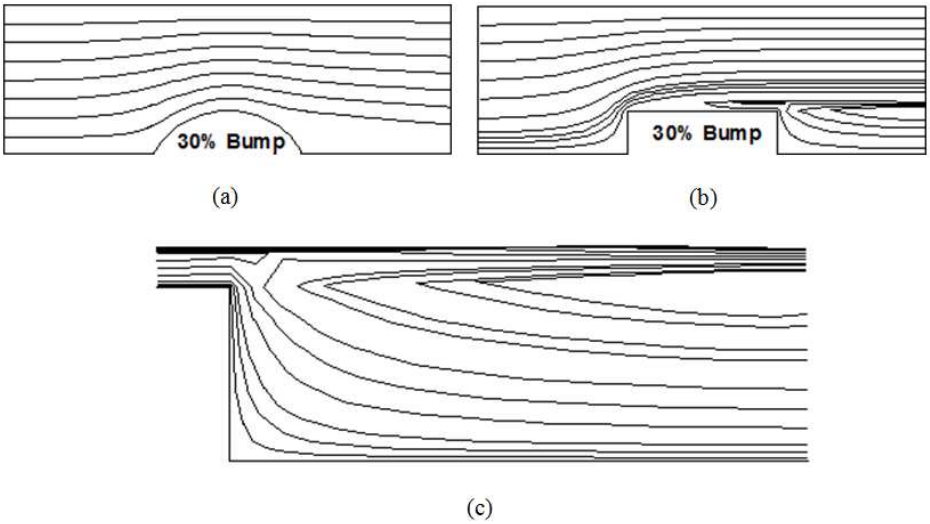

Fig 9. *Streamline plot along the channel with a) 30% arc circular bump b) 30% rectangular bump c) zoomed in view of the secondary flow within the channel with 30% rectangular bump*

The thermodynamic influence of secondary flow has been investigated in the fig 10, in which the secondary flow streamlines have been superimposed onto a contour plot of the variance of density (kg/m^3) within the channel.In the fig.10 it can be easily observed that there is no evidence of expansion or contraction of the fluid flow in the vicinity of the recirculatory region. Such variance of density in this region is paramount to support thetheory of secondary flow acting as a refrigeration loop. The reason being that for any compressible fluid, density variance is related to temperature according to the ideal gas law of Equation (2).As this is the case not only for density but alsofor the static temperature and static pressure contour plots shown belowin Fig. 11 and 12, it can be now observed that there is no variation of these variables intandem with secondary flow in the region, sufficient to prove Ahlbornetal.'s[12] refrigeration theory.These results are completely in agreement with the ones in Ronan [13].

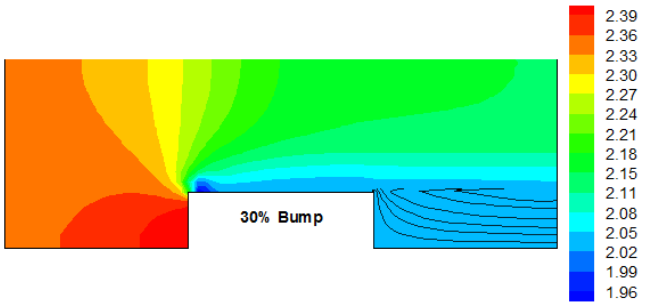

Fig 10. *Density contour plot along the channel with 30% rectangular bump*

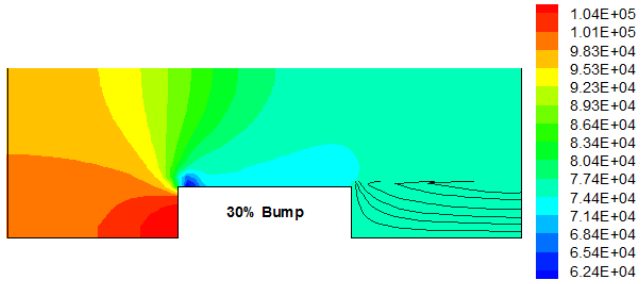

Fig 11. *Static pressure contour plot along the channel with 30% rectangular bump*

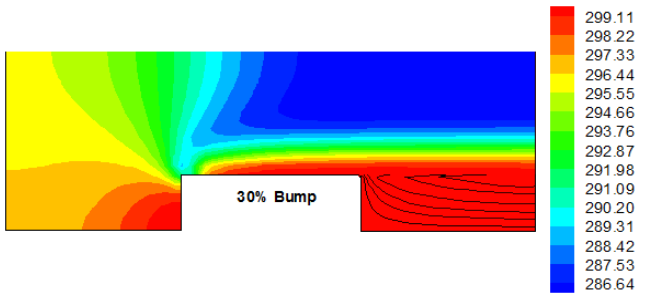

Fig 12. *Static temperature contour plot along the channel with 30% rectangular bump*

6. Conclusion

In the present article, by using Computational Fluid Dynamics technique and Finite Volume method, the flow field manner throughout a rectangular channel with both arc circular and rectangular bump having height as high as 10%, 30% and 50% of total channel height was investigated. For

all studied cases the inlet Mach number considered 0.5 and the effect of geometry of bump on the air flow behavior in the channel was studied. The flow inside the channel (air) was considered compressible, steady, isentropic and 2 dimensional. The results show a more regular distribution of Mach number and static pressure for circular bumps than rectangular ones. The maximum Mach number on the lower wall increases due to increasing the height of bump for the arc circular bumps and in contrastdecreases for rectangular bumps.The same results were obtained for the Mach number distribution along the centerline. The Mach number investigation demonstrates the propriety of 30% circular bump for usage because of higher exit velocity. The static pressure is higher in the front part of bump in all cases. In addition, the velocity vector investigation displayed a secondary back flow for rectangular bump models at the back region of bump which is not occurred in arc circular models. The streamlines throughout the channel confirmed this phenomenon. Secondary flow existence causes to observe no evidence of expansion or contraction of the fluid flow in the vicinity of the recirculatory region and the same manner was occurred during the investigation of static temperature and pressure. Such variance of thermodynamics properties in this region is paramount to support thetheory of secondary flow acting as a refrigeration loop.

Nomenclature

a - The speed of sound
K - Heat conduction coefficient
M - Molecular mass
Ma - Mach Number
P - Pressure
$\overline{R}$ - Universal gas constant
Re - Reynolds number
t - Time
T - Temperature
V - Speed

Greek Symbols

γ - Ratio of the specific heats
ρ - Density
μ - Viscosity

References

[1] Mallet M (1985) A finite element method for computational fluid dynamics. Ph.D Thesis, Stanford University.

[2] Shapiro R (1988) An adaptive finite element solution algorithm for the Euler equations. Ph.D Thesis, Massachusetts Institute of Technology.

[3] Le Beau GJ, Tezduyar TE, (1991) Finite element computation of compressible flows with the SUPG formulation. Advances in Finite Element Analysis in Fluid Dynamics ASME 123:21-27.

[4] Djavareshkian MH, (2004) Pressure-based compressible calculation method utilizing normalized variable diagram scheme. Iranian Journal of Science & Technology, Transaction B 28(4):495-500.

[5] Rizzi AW, (1981) Numerical methods for the computations of transonic flows with shock waves. Notes on Numerical Fluid Mechanics, Vieweg, Braunschweig 3.

[6] Veress A, (2001) Incompressible flow solver by means of Pseudo-Compressibility method. HEJ, ANM-030110-A:1-10.

[7] Sandham ND, Yao YF, Lawal, AA, (2003) Large-eddy simulation of transonic turbulent flow over a bump. International Journal of Heat and Fluid Flow 24:584-595.

[8] Chiocchia G, Gabutti B, (1989) A new transformation for computing hypergeometricseries and the exact evaluation of the transonic adiabatic flow over a smooth bump. Computers & Fluids 17(1):13-23.

[9] Wong WS, Qin, N, Sellars N, Holden H, Babinsky H, (2008). A combined experimental and numerical study of flow structures over three-dimensional shock control bumps. Aerospace Science and Technology 12:436-447.

[10] Darwish MS, Moukalled F, (1994). Normalized variable and space formulation methodology for High-Resolution schemes. Numerical Heat Transfer 26:79-96.

[11] Graebel WP (2007) Advanced Fluid Mechanics. 1st Edition, Elsevier, Burlington.

[12] Ahlborn B, Gordon J, (2000) The vortex tube as a classical thermodynamic refrigeration cycle. Journal of Applied Physics 88(6): 645-653.

[13] Ronan O, (2008) Numerical prediction of primary and secondary flows in a Ranque-Hilsch vortex tube. MS Thesis, Dublin Institute of Technology.